Beryllium(II): The Strongest Structure-Forming Ion in Water? A QMCF MD Simulation Study

S. Sikander Azam, Thomas S. Hofer, Anirban Bhattacharjee, Len Herald V. Lim, Andreas B. Pribil, Bernhard R. Randolf, and Bernd M. Rode*

Theoretical Chemistry, Division, Institute of General, Inorganic and Theoretical Chemistry University of Innsbruck, Innrain 52a, A-6020 Innsbruck, Austria

Received: April 17, 2009; Revised Manuscript Received: May 22, 2009

A quantum mechanical charge field (QMCF) molecular dynamics (MD) simulation including the first and second hydration shells in the QM region has been carried out to describe the structural and dynamical properties of Be^{2+} in aqueous solution. In this methodology, the full first and second hydration shells are treated by *ab initio* quantum mechanics supplemented by a fluctuating electrostatic embedding technique. From the simulation, structural properties were extracted and were found to be in good agreement with previously published experimental and theoretical results. The radial distribution function (RDF) showed the maximum probability of the Be−O bond length at 1.62 Å. The first tetrahedrally arranged hydration shell is highly inert with respect to ligand-exchange processes. Application of local-density-corrected three-body correlation analysis showed minor structural influence of the ion beyond the second hydration layer, contrary to the findings of a previous QM/MM MD simulation. The dynamics of the hydrate were studied in terms of ligand mean residence times (MRTs) and the power spectrum of the Be^{2+}−O stretching frequency. A comparison of the "classical" QM/MM framework with the QMCF method clearly demonstrated the advantages of the latter, as ambiguities arising from the coupling of the subregions occurring in QM/MM MD simulations did not appear when the QMCF ansatz was applied.

1. Introduction

Beryllium is a naturally occurring metal that is found in beryl and bertrandite rock and is well-known for its toxicity in mammals.[1,2] Beryllium has very specific physicochemical properties, including low density, high melting point, and high tensile strength of its alloys, that make it useful in the manufacture of products ranging from space shuttles to golf clubs.[3,4] It is a good neutron moderator, and because of its low weight and high rigidity, it is utilized as a material for high-frequency drivers in acoustics. Beryllium-containing materials have gained high importance in many key technologies including nuclear fission and nuclear fusion; radiation sources; high-temperature ceramics for microelectronics; and high-performance alloys for naval, aircraft, and space technologies.[4−6] The best known health hazard related to beryllium is chronic beryllium disease (CBD),[7,8] but Be can also cause contact dermatitis, and beryllium and its compounds are carcinogenic for both animals and humans.[9] Beryllium's most fascinating form is emerald, a beryllium−aluminum silicate whose luminous color makes it a precious gemstone. Despite the importance of this element, the chemistry of beryllium is relatively unexplored compared to that of its neighboring elements[10] because of a growing concern about the toxicity of this element and its compounds, which has discouraged basic research on beryllium and even industrial activities.[1,9,11,12] Most industrial chemistry of beryllium, and its toxicity, is based on equilibria in aqueous solutions.[1,2] Therefore, detailed knowledge of the behavior of the Be^{2+} ion in aqueous solution, including a description of its structure-forming effects, is desirable. For a structure-making ion, the ordering of the bound water molecules must outweigh the order of the solvent structure. Such ions will be highly polarizing, and therefore, in particular, small and/or highly charged metal ions such as Li^+, Mg^{2+}, Al^{3+}, and first-row transition-metal ions are considered strong structure formers. On the other hand, larger and/or less polarizing ions such as Rb^+ and Cs^+ exhibit structure-breaking effects.[13,14] Various experimental techniques [X-ray diffraction, neutron diffraction (ND), Raman spectroscopy, IR spectroscopy][15−22] have yielded a tetrahedral first hydration shell structure for Be^{2+} in aqueous solution with ion−oxygen distances varying from 1.61 to 1.67 Å. An early classical MD simulation of $BeCl_2$ in aqueous solution gave an average first-shell distance of 1.75 Å with coordination number 4.[17] A Car−Parrinello MD simulation[23] produced an r_{max} value of 1.65 Å for the first shell with a coordination number of 4, with the second shell appearing very tight. These effects can be attributed to the small periodic box of about 10 Å containing 31 water molecules, which does not provide realistic surroundings for the second hydration shell. The different first-shell distances obtained from various simulation techniques are compared in Table 1. Current advancements in computational capacities open the way to utilizing more sophisticated simulation techniques using combined quantum mechanical and molecular mechanical (QM/MM) simulations[24−28] to resolve such differences and ambiguities concerning the influence of an ion on the surrounding solvent, and in this context, an extended *ab initio* QM/MM MD simulation has been performed on Be^{2+} in aqueous solution.[29] The recently developed quantum mechanical charge field (QMCF) approach for the treatment of solvated systems further enhances the capabilities of this methodology.[30,31] This approach does not require the construction of any other potential functions except those for solvent−solvent interactions while maintaining all of the advantages of large simulation boxes and ensuring the accuracy

* To whom correspondence should be addressed. E-mail: Bernd.M.Rode@uibk.ac.at. Tel.: +43-512-507-5129. Fax: +43-512-507-2714.

10.1021/jp903536k CCC: $40.75
Published on Web 06/12/2009

TABLE 1: Maxima (r_M) and Minima (r_m) of the Be−O and Be−H Radial Distribution Functions and Average Coordination Numbers CN_{av} of First, Second, and Third Hydration Shells Obtained from Various Simulations and Experiments

method	r_{M1} (Å)	r_{m1} (Å)	$CN_{av,1}$	r_{M2} (Å)	r_{m2} (Å)	$CN_{av,2}$	r_{M3} (Å)	r_{m3} (Å)	$CN_{av,3}$
				Be−O					
QMCF MD[a]	1.62	1.9	4	3.75	4.5	9.0	−	−	−
QM/MM MD[29]	1.63	1.9	4	3.7	4.5	9.2	5.4	6.0	19
$BeCl_2$ CMD[17]	1.75	2	4	4.4	5.1	25	6.4	7.5	−
Be^{2+} CPMD[23]	1.65	1.9	4	3.9	4.3	9	−	−	−
Be^{2+} CMD[62]	1.65	2.1	4	3.9	4.5	9	5.8	6.8	−
Be^{2+} MD[69]	1.72	−	4	4.5	−	−	−	−	−
X-ray, IR[15,17−22]	1.610−1.67	−	4	−	−	9 (8)	−	−	−
ND[16,70]	1.6	−	4	−	−	−	−	−	−
				Be−H					
QMCF MD[a]	2.2	2.6	8	4.35	5.0	21	−	−	−
QM/MM MD[29]	2.3	2.6	8	4.2	5.0	23.5	6.2	6.7	47
$BeCl_2$ CMD[17]	2.5	2.75	8	4.6	5.6	−	6.8	7.7	−
Be^{2+} CPMD[23]	2.37	2.7	8	4.1	4.5	17	−	−	−
Be^{2+} CMD[62]	2.36	2.8	−	4.5	5.0	−	6.5	7.4	−

[a] This work.

of *ab initio* quantum mechanics for all forces acting in a larger relevant region without introducing the inherent ambiguities of the fitted ion−solvent potentials.[30] The present work aims to make use of this improvement to obtain detailed insight into the structure and dynamics of Be^{2+} in aqueous solution at the highest level of accuracy affordable with present computational facilities.

2. Methods

2.1. Simulation Method. One of the most critical steps in performing a quantum chemical study is the selection of suitable basis sets. In *ab initio* geometry optimizations in this work, a modified LANL2DZ basis set was used, which produced structural properties that compared well with previous investigations and test calculations performed by D'Incal et al.[29] For O and H, Dunning double-ζ plus polarization basis sets were employed.[32] The choice of a proper quantum mechanical level for calculations is also an essential factor in determining the accuracy and computation time, as well as the correctness of dynamical results.[33] Previous QM/MM and QMCF MD simulations of ionic solutes[29,34,35] have yielded data in good agreement with experimental measurements when the *ab initio* Hartree−Fock (HF) method utilizing at least double-ζ plus polarization basis sets was employed. On the other hand, density functional theory (DFT) methods have typically yielded results different from both experimental data[14,29,36,37] and correlated *ab initio* methods[14,38−44] for ion−water systems. To estimate the methodical reliability, geometry optimizations of Be^{2+} clusters with between one and six water molecules have been performed at different levels of theory in connection with previous QM/MM MD simulations of Be^{2+} in aqueous solution,[29] confirming the HF level as a good compromise between effort and accuracy.

Both QM/MM approaches[24−28] and the QMCF methodology[30,31,45] utilize a partitioning scheme in which the system is divided into two parts, whereby the chemically most relevant region, the ion and its immediate vicinity, is treated by *ab initio* quantum mechanics while the remaining part of the system is taken into account by empirical potentials. Differences between the two methodologies and advantages of the QMCF MD approach have already been extensively discussed in previous publications.[30,31] Thus, the QMCF framework offers a straightforward route to access any kind of solutes such as metal complexes and even composite solute species.[35,46−50]

2.2. Structural Evaluation. The most basic analysis performed to obtain insight into structural attributes is the site−site radial pair distribution function (in this case, Be−O and Be−H pair distribution functions). One particular advantage of the pair distribution function is that it can also be directly obtained from experimental methods.[51] To retrieve precise information concerning the geometry of the first hydration shell, the corresponding O−Be−O angular distribution functions were also calculated. Two additional angles were investigated in order to describe the orientation of water ligands relative to the ion. The tilt angle is defined as the angle between the ion−O vector and the plane formed by the two O−H vectors, and θ is the angle between the ion−O vector and the sum of the two O−H vectors.

In principle, because all information about particle positions is available in the simulation trajectory, one can expand from two-particle to three-particle correlations in order to observe the system from the point of view of a solvent particle. In this manner, local reorganizational attributes can be measured, allowing more information to be obtained on solvation structures. The phenomena of solvation can also be viewed from another interesting aspect, which is the reorganization of solvent molecules in different solvation layers. A solvent such as water itself has a hydrogen-bonded structural network that can be deduced from O−O and O−H radial distribution functions. When a strongly interacting solute is inserted into the existing structural framework of the solvent, it influences the solvent structure in its vicinity. The solvent−solvent pair distribution functions are not significantly responsive to such local structure reorganizations, as the majority of the contributions result from the solvent particles residing in the bulk, where no reorganization takes place. The three-body correlation function [$g^{(3)}_{X-O-O}(s,r,s)$; see Figure 1],[52,53] which accounts for deviations from an ideal system in terms of the number of triples, is very well suited to investigate solvent reorganization in the vicinity of a solute.[54] The three-body correlation function measures the distribution of any two solvent particles in relation to the solute inside a spherical volume element defined by $s \pm \Delta s/2$. The value of $g^{(3)}_{X-O-O}$ for any given triple (s,r,s) is defined as the probability of finding a solvent−solvent distance of r within the volume element $s \pm \Delta s/2$. It is obvious that the absolute magnitude is directly related to the local density introduced by the presence of the solute and the respective distribution of solvent molecules. To obtain information about the solvent structure in a given solvation shell, the local-density-corrected three-body distribution function, $f^{(3)}_{X-O-O}(s,r,s)$, was calculated.[54] $f^{(3)}_{X-O-O}(s,r,s)$ enables a direct comparison of the local solvent structure

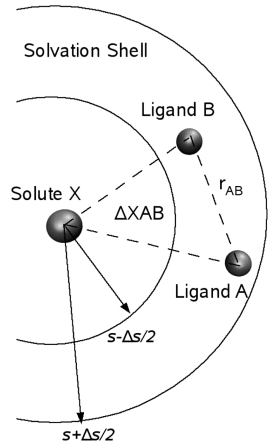

Figure 1. Scheme for probing reorganizations of local solvent structure in terms of three-body distributions $g^{(3)}_{X-O-O}(s,r,s)$.

reorganization of a given shell. The final form of the equation is given by

$$f^{(3)}_{X-O-O}(s,r,s) = \frac{\langle N^{(3)}(s,r,s)\rangle}{8\pi^2 N_X \rho_{Shell}{}^2 r s^2 \Delta s^2 \Delta r} \quad (1)$$

where $\langle N^{(3)}(s,r,s)\rangle$ represents the average number of ion−O−O triples with ion−oxygen distances lying in the range of $s \pm \Delta s/2$. ρ_{Shell} is given by the equation

$$\rho_{Shell} = \sqrt{N_{Shell}(N_{Shell} - 1)/V_{Shell}{}^2} \quad (2)$$

2.3. Evaluation of Dynamics. From the knowledge of particle positions at each time point in the simulation trajectory, the mean residence times (MRTs) can be computed utilizing the direct method[55] by counting the number of successful ligand exchanges. The parameter t^* determines the minimum time span for a ligand displacement from its original coordination shell to be considered successful and was set to 0.5 ps. This time interval also corresponds to the experimental mean lifetime of H-bonds in water.[56] Mean residence times τ in picoseconds evaluated for t^* values of 0.0 and 0.5 ps are represented by $\tau^{0.0}$ and $\tau^{0.5}$, respectively, in Table 2. The sustainability of exchange processes can be defined as

$$S_{ex} = \frac{N^{0.5}_{ex}}{N^{0}_{ex}} \quad (3)$$

where S_{ex} is the sustainability coefficient, N^0_{ex} is the number of all transitions through a shell boundary ($t^* = 0.0$), and $N^{0.5}_{ex}$ denotes the number of exchanges persisting longer than 0.5 ps. Its inverse (R_{ex}) counts how many attempts are required, on average, to produce one lasting exchange between the hydration shells and the bulk.

In addition to the evaluation of dynamical properties through parameters such as water exchange rates and mean residence times of ligand molecules, in the current work, the ion−oxygen stretching frequency was also evaluated using velocity autocorrelation functions (VACFs), $C(t)$, defined as

$$C(t) = \frac{\sum_{i}^{N_t}\sum_{j}^{N} \vec{v}_j(t_i)\,\vec{v}_j(t_i + t)}{N_t N \sum_{i}^{N_t}\sum_{j}^{N} \vec{v}_j(t_i)\,\vec{v}_j(t_i)} \quad (4)$$

where N is the number of particles, N_t is the number of time origins t_i, and $\vec{v}_j$ denotes a given velocity component of the particle j. The power spectrum of the VACF was calculated by Fourier transformation, using a correlation length of 2.0 ps with 2000 averaged time origins. Because of the rather constant systematic errors of the Hartree-Fock frequencies, the standard factor of 0.89 was applied to scale all frequencies obtained by the QMCF MD simulation.[57,58]

2.4. Simulation Protocol. A pre-equilibrated elementary cubic box with a side length of 24.6 Å containing one ion immersed in 499 water molecules was utilized as the starting structure. The density of the system corresponded to that of the pure solvent at 298 K (0.997 g/cm^3). Periodic boundary conditions were applied, and the canonical (NVT) ensemble was chosen, with temperature controlled by the Berendsen algorithm.[59] An Adams−Bashforth predictor−corrector algorithm was used to integrate the Newtonian equations of motion with a time step of 0.2 fs. The cutoff distances for non-Coulombic interactions were set to 5.0 and 3.0 Å for O−H and H−H interactions, respectively. For the Coulombic interactions, a cutoff of 12.0 Å was set, and the reaction field method was used to correct the errors associated with this cutoff. For water, the flexible BJH-CF2[60,61] potential was employed, as its intramolecular term ensures the full flexibility of water molecules indispensable for correct transition between the QM and MM regions.

TABLE 2: Ion Radius (r_{ion}) and Charge-to-Radius Ratio ($r_{q/r}$), Maxima (r_M) and Minima (r_m) of the Ion−O Radial Distribution Functions, and Average Coordination Numbers ($CN_{av,1}$) of the First Hydration Shell Obtained from Various Simulations, as Well as Mean Residence Times (τ) Evaluated by the Direct Method for t^* Values of 0.0 and 0.5 ps, Including Values Obtained from the QM/MM MD Simulation of Pure Water

Radial Distribution Functions and Coordination Numbers

ion (method)	r_{ion} (Å)	$r_{q/r}$ (e/Å)	r_{M1} (Å)	r_{m1} (Å)	$CN_{av,1}$	r_{M2} (Å)	r_{m2} (Å)
Mg^{2+} (QM/MM)[71]	1.72	3.5	2.03	2.47	6.0	4.12	4.68
Al^{3+} (QMCF)[45]	1.82	5.5	1.88	2.2	6.0	4.15	4.85
Al^{3+} (QM/MM)[38]	1.82	5.5	1.86	2.1	6.0	4.10	4.75

Mean Residence Times

ion (method)	shell	$\tau^{0.0}$ (ps)	$\tau^{0.5}$ (ps)	R_{ex}[a]	CN[b]
Mg^{2+} (QM/MM)[72]	second	0.47	4.2	9.0	14.0
Al^{3+} (QM/MM MD)[73]	second	1.8	26.4	15	12.2
Al^{3+} (QMCF MD[45])	second	0.84	17.7	21.1	12.8
Be^{2+} (QM/MM MD)[29]	second	0.4	4.8	10.0	9.2
Be^{2+} (QMCF MD)	second	0.31	3.9	14.2	9.0
H_2O (QM/MM MD)[64]	−	0.33	1.5	4.6	4.1

[a] Number of migration attempts needed to achieve one sustainable exchange. [b] Coordination number.

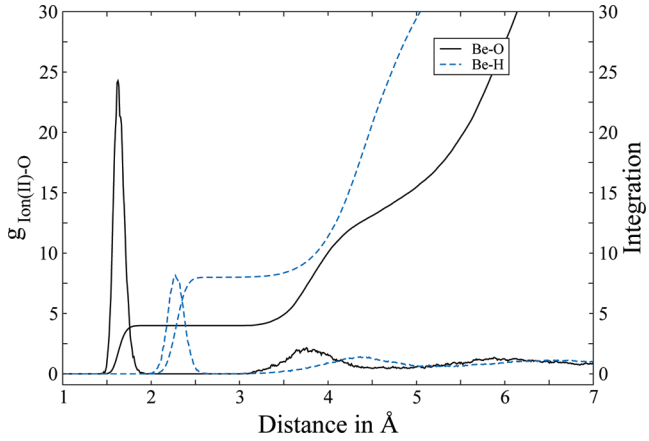

Figure 2. Be−O (solid line) and Be−H (dashed line) RDFs and running integration numbers obtained from the QMCF MD simulation.

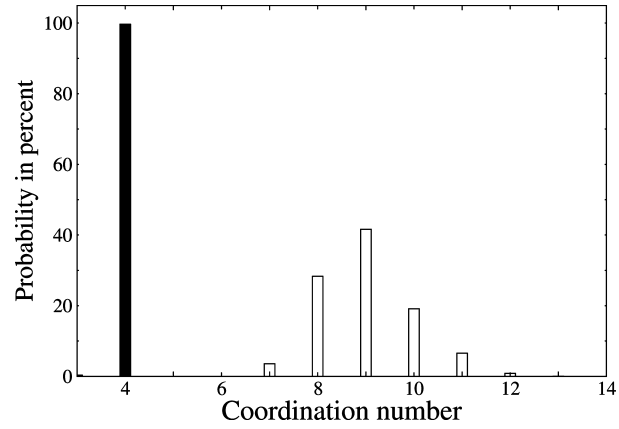

Figure 3. First- and second-shell coordination number distributions for Be^{2+} obtained from a QMCF MD simulation.

The QMCF MD simulation was performed using the equilibrium configuration obtained from a preliminary QM/MM MD simulation, which included the ion and its first hydration shell in the QM region. The simulation was sampled for 12 ps after 3 ps of equilibration. The total radius of the QM region was set to 6.0 Å. The splitting of the QM region at a radius of 2.0 Å ensures the inclusion of the full first coordination shell within the core region, and the smoothing function was applied in the region from 5.8 to 6.0 Å. The Mulliken population analysis scheme was chosen as the most suitable population analysis scheme for obtaining partial charges during the simulation, as it delivers point charges of water molecules near the outer surface of the layer region that are compatible with the BJH-CF2 fixed point charges. Instead of using fixed point charges, fluctuating point charges obtained by applying a suitable population analysis scheme lead to a more realistic description of the Coulombic interactions between the QM and MM regions.

3. Results and Discussion

The Be^{2+}−O radial distribution functions (RDFs) obtained from the QMCF MD simulation agree well with the previous investigation including two hydration shells in the QM region.[29] The maximum of the first peak in the RDF, corresponding to the nearest ligands in the first hydration shell, is located at 1.62 Å (see Figure 2). Two distinct hydration layers are observed, and the characteristic data are listed in Table 1. The border between the first and second shells was determined as 1.9 Å. Because no exchange of first-shell ligands took place during the entire simulation, the first-shell coordination number remained fixed at 4. In addition to the first-shell distance and the coordination number, the half-width and intensity of the first-shell peak are sensitive indicators to quantify hydration structures. The half-width of the first-shell peak of the Be^{2+}−O RDF obtained from the QMCF MD simulation was 0.135 Å, and for the Be^{2+}−H RDF, a value of 0.235 Å was observed. This indicates the presence of a rigid first hydration shell. The peak maximum of the second hydration shell was at a distance of 3.7 Å. Integration of the RDF up to the subsequent minimum at 4.5 Å yielded a coordination number of 9.0. The results of the QMCF MD simulation are in excellent agreement with experimental data from different techniques[15−17] yielding first-shell distances between 1.61 and 1.67 Å with a coordination number of 4 and a second-shell coordination number of 9.0 (see Table 1 for comparison). Based on the coordination number distribution, the mean value of the second-shell coordination number was determined to be 9.36 with a standard deviation of ± 1.2. The third hydration layer was not well-defined, although a slight ordering effect was observed beyond the second shell, and no experimental data are available for a defined third hydration layer for Be^{2+} in aqueous solution. In a previous QM/MM MD study,[29] a third shell was distinguished that might be due to an artifact in the smoothing region.

The coordination number distributions of hydrated Be^{2+} obtained from the QMCF MD simulation are shown in Figure 3 for the first and second hydration layers, obtained by setting the shell borders according to the ion−oxygen RDF. A constant coordination number of 4 observed for the highly stable first hydration shell reaffirms the rigidity of this shell, coinciding with most of the values obtained from theoretical evaluation and experiments (see Table 1). The second hydration shell displays a distribution of coordination numbers ranging from 7 to 12 with a maximum at 9. This 9-fold coordination matches with the experimental results obtained from X-ray and IR studies,[15,17−22] as well as other simulations[23,62] (Table 1). A third hydration layer was not clearly observed in the QMCF MD simulation, reflecting a rapid exchange of ligands between the second shell and the bulk.

Hydration structures can be discussed further on the basis of angular distribution functions (ADFs). Figure 4a displays the O−Be−O angular distributions within the first shell from 0.0 to 1.9 Å, and Figure 4b shows the distribution within the second shell ranging from 1.9 to 4.5 Å. The maximum observed and the angle distributions of Be^{2+} obtained from the QMCF MD simulation are closer to the values for a tetrahedron than are those of Li^+, which has a similar coordination number of 4 and a maximum O−Li−O angle observed at 101°. Thus, the distribution emphasizes the compactness of the first shell of Be^{2+}, with the ADF confirming the tetrahedral geometry as the main structural motif as depicted by the snapshot in Figure 5. The shape of the distribution for the second shell displays the relative structural lability of this hydration sphere.

The tilt distribution within the first shell starts at −64° and ends at +64°, having its maximum at about −2.2°, whereas that for the second shell starts at −90°, ends at +90°, and has a maximum at approximately −15°, as depicted in Figure 4c,d. The observed tilt maximum indicates that water dipoles are highly aligned with the ion−O axis. Noticeably, the first-shell maximum obtained from the QM/MM MD simulation of Be^{2+} in aqueous solution[29] indicated a slightly weaker interaction of the ion with solvent compared to what was observed from the QMCF MD simulation, which seems to be a consequence of the better description by fluctuating charge interactions between

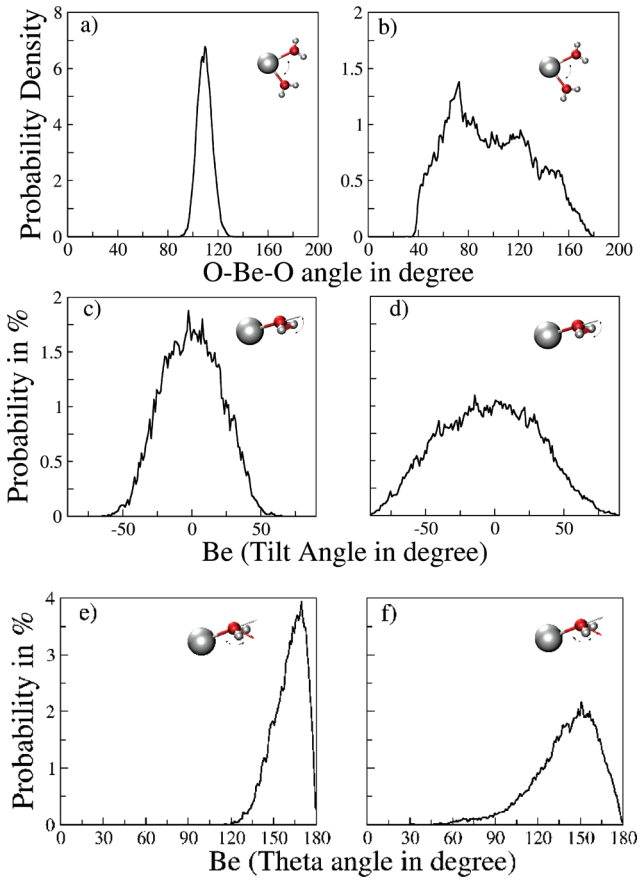

Figure 4. Comparison of the distributions of the (a,b) O−ion−O angle, (c,d) tilt angle, and (e,f) θ angle within (a,c,e) first and (b,d,e) second shells for Be^{2+} in aqueous solution obtained from a QMCF MD simulation. The model structures are the schematic representations of respective angular distributions.

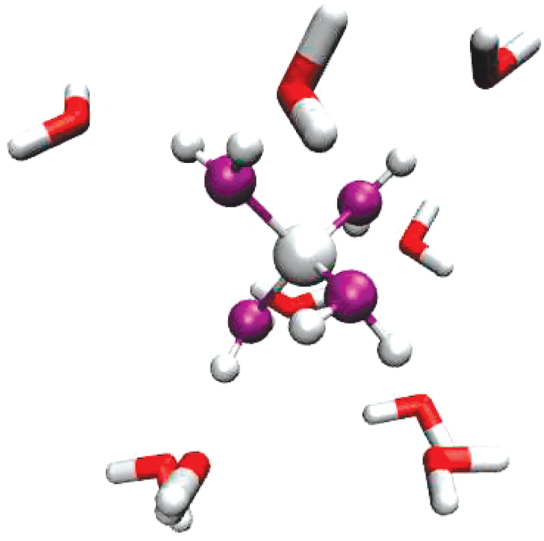

Figure 5. Snapshot showing the 4-fold (purple) and 9-fold (red) coordination environments for the first and second shells, respectively, for Be^{2+} obtained from the QMCF MD simulation.

the QM and MM regions in the QMCF methodology. A similar reduced angular flexibility has also been observed for Al^{3+} [45] upon the application of the QMCF methodology. The θ angle distribution (Figure 4e,f) has a peak at ∼170° with a tailing toward 115° in the first-shell region, and the corresponding values for the second shell are ∼150° and ∼40°, respectively. The values indicate a limited orientational freedom for water molecules within the first shell. These distributions are similar to those of other divalent ions such as Mg^{2+}.[63]

Figure 6b displays the local-density-corrected three-body distribution[54] of the first hydration shell of Be^{2+}, exhibiting only one sharp peak at 2.65 Å. The single sharp peak suggests that the four oxygen atoms are equidistant from one another. The tetrahedral structure can also be depicted by the peak position in Figure 6b. Precisely, given a first-shell Be−O distance of 1.62 Å, for a tetrahedral geometry, the first-shell peak should appear at 2.65 Å (corresponding to 1.633a, where a = 1.62 in the present case; cf. Figure 6a). The predicted peak position matches perfectly with the one observed. This again confirms the highly regular 4-fold coordination of the first solvation shell.

The comparative analysis of the second-hydration-shell structures (cf. Figure 6c) was done by utilizing the O−O radial pair distribution of pure water obtained from a QM/MM MD simulation[64] as the reference solvent structure where the second hydration shell has been included in the QM region. It can also be deduced from the local-density-corrected distribution functions [$f^{(3)}_{Be-O-O}(s,r,s)$] that a well-structured second hydration shell is present with a peak maximum found at 4.5 Å that is more pronounced in the results obtained from the QMCF MD simulation than those from the QM/MM MD simulation.[29] This also indicates that a more pronounced structural influence in the second hydration shell is observed upon the application of QMCF framework, which better accounts for the polarizability of the ion and the ligands in the QM region.

In Figure 6d, the presence of a slight structural order beyond the second shell of Be^{2+} can be identified with that of the O−O RDF of pure classical water obtained using BJH-CF2 model,[60,61] as this region is located outside the QM zone. In this bulk region, differences are visible giving a clear indication of the influence of the Be^{2+} ion beyond the second hydration shell. The behavior of the three-body correlation function is quite interesting in this part. The first peak, well-reduced in intensity but corresponding to the same position of the O−O radial pair distribution function, somehow indicates the onset of the original water structure, although differences in the rest of the curve give a clear indication of an existing structural influence of the Be^{2+} ion in this region (i.e., beyond the second solvation shell), which, however, is not strong enough to form a distinct third hydration layer, in contrast to the previous QM/MM MD simulation.[29] The ion's weak ordering effects beyond the second shell, however, emphasizes the strong structure-forming behavior of this ion in aqueous solution.

A comparative analysis (see Table 2) shows that Al^{3+}, Be^{2+}, and Mg^{2+}, which have not been found to show any ligand exchange in their first hydration shells, share a common trait: relatively high charge-to-radius ratio, in the order Mg^{2+} (3.5) < Al^{3+} (5.5) < Be^{2+} (5.7).[13,45,65] These ions attract nearby ligands tightly, leading to a well-structured first hydration shell, and are thus known as the strongest structure formers. The dynamical behavior of the system was characterized by evaluation of the ion−oxygen stretching frequency. The frequency was multiplied by the standard factor of 0.89.[57,58] The scaled average frequency of the Be^{2+}−O stretching mode is 653 cm^{-1}, corresponding to a force constant for the Be−O bond of 144 N m^{-1}, which is much higher than the values for other divalent ions such as 97 N m^{-1} for Mg^{2+},[63] 46 N m^{-1} for Ca^{2+},[66] 73 N m^{-1} for Zn^{2+},[34] and 86 N m^{-1} for Fe^{2+} [67] (see Table 3). The force constant obtained for Al^{3+} (194 N m^{-1}), however, indicates an even stronger ion−water bond than in hydrated Be^{2+} but still assigns a similar polarizing strength to this divalent ion as for the trivalent Al^{3+}.

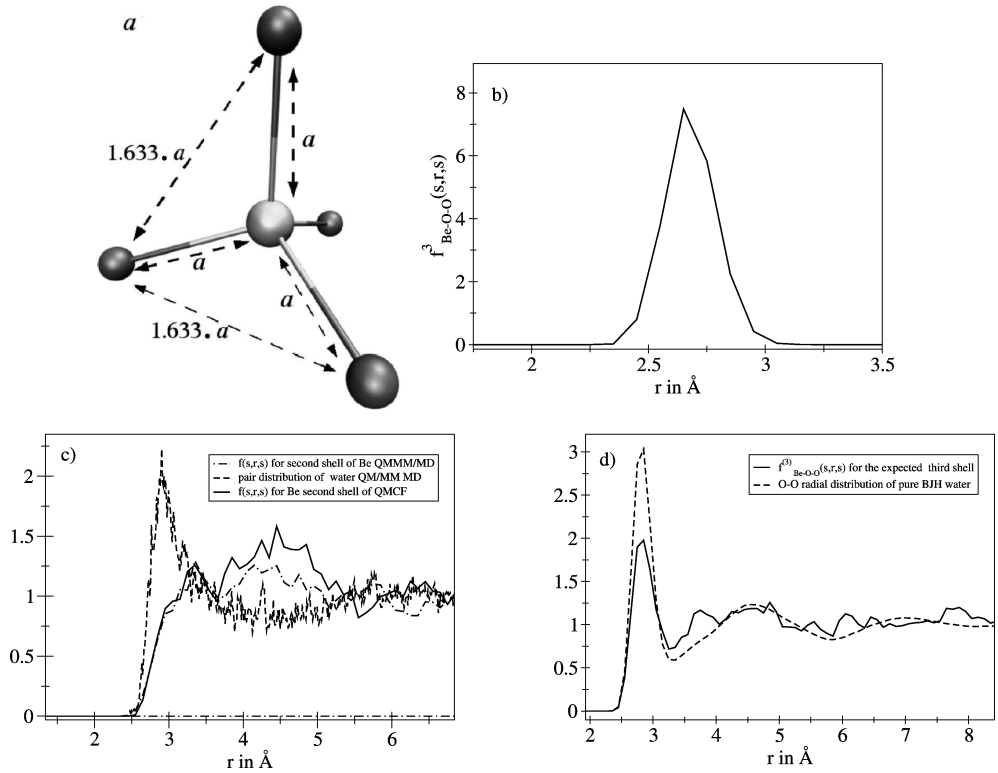

Figure 6. (a) Basic scheme for obtaining ligand−ligand distances in tetrahedral geometries. (b) $f^{(3)}_{Be-O-O}(s,r,s)$ for the first hydration shell of Be^{2+} in aqueous solution. Comparison of the (c) second and (d) third shells of the Be^{2+} and O−O radial distribution functions of pure water in terms of the local-density-corrected three-body distribution.

TABLE 3: Peak Maximum of the Ion−Oxygen Stretching Frequencies (Q_{ion-O}) and Corresponding Force Constants (k_{ion-O}) Obtained from QM/MM and QMCF MD Simulations of Different Ions

ion	method	Q_{ion-O} (cm^{-1})	k_{ion-O} (N m^{-1})
Mg^{2+}	QM/MM[a 72]	–	97
Al^{3+}	QM/MM MD[a 73]	520	160
Al^{3+}	QMCF MD[45]	560	194
Be^{2+}	QM/MM MD[a 29]	658	147
Be^{2+}	QMCF MD[a]	653	144
Ca^{2+}	QM/MM MD[a 66]	260	46
Zn^{2+}	QM/MM MD[a 34]	310	73
Fe^{2+}	QM/MM MD[a 67]	342	86

[a] Value scaled by a factor of 0.89.[74,75]

A further elaboration of the structure-forming ability can be achieved on the basis of ligand mean residence times for the second shell. Comparing the MRT values for the strongly polarizing ions Be^{2+}, Mg^{2+}, and Al^{3+}, which are 4.8, 4.2, and 17.7 ps, respectively (cf. Table 2), it seems obvious that the structure-forming effect of Al^{3+} is by far the strongest outside the first shell, despite the slightly higher charge/radius ratio of Be^{2+}, which has been a basis for the assumption that this ion is the strongest structure former. The value of R_{ex} (i.e., the number of attempts needed to achieve one successful exchange) also clearly confirms the higher stability of the second hydration shell of Al^{3+} compared to that of Be^{2+}. The average coordination numbers of the second shell are $2N + 1$ for both ions, where N is the first-shell coordination number. This means that each first-shell ligand is strongly connected to two s-shell ligands in a rather stable structure. All ions considered in this comparison have a quite stable second shell, even Mg^{2+}, whose MRT is still more than 3 times higher than that of pure water. Small cations, with high q/r ratios, cause strengthening of hydrogen bonds, and they shift the OD band toward lower frequencies in IR spectra where the Al^{3+} first and second shells lie in the ranges of 2200 ± 20 cm^{-1} and 2420 ± 20 cm^{-1}, respectively.[68] These values correspond to water molecules experiencing a severe electrostriction effect and forming very strong hydrogen bonds between the first and second hydration shells and between the second and third hydration spheres of this trivalent cation. Summarizing the results, one can clearly state that Be^{2+} is not the strongest structure-forming ion in solution, but that force constant, MRT, and exchange characteristics confirm Al^{3+} to assume this position. The contrast to the order of charge/radius ratios has its cause in ligand−ion charge-transfer effects, which are fully reflected in the QMCF methodology. Figure 7 shows the fluctuation of the actual charge on the Be^{2+} ion, which varies from +1.05 to +1.25, and hence leads to a strongly reduced charge/radius ratio as well.

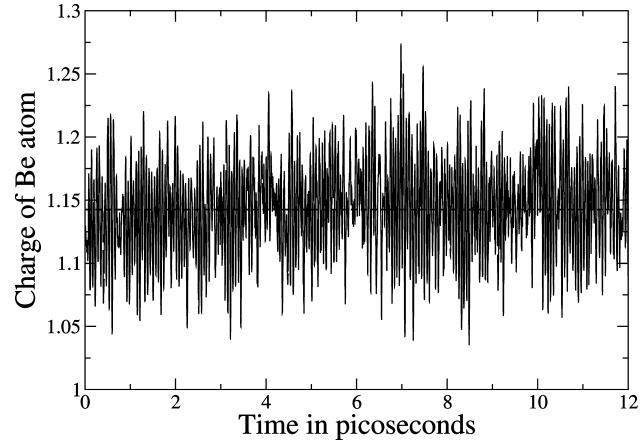

Figure 7. Partial charges deduced from the QMCF MD simulation for a Be atom with respect to the simulation time. The dashed line shows the mean value around which the total charge fluctuates.

4. Conclusion

This simulation study on hydrated Be^{2+} ion utilizing the improved QMCF framework has yielded a variety of information. Comparison with the conventional QM/MM approach as well as some classical methods has emphasized the advantages of the new methodology, which, upon inclusion of the fluctuating electrostatic embedding technique, results in a more adequate quantum mechanical treatment. Structural findings confirm an exclusive 4-fold tetrahedrally coordinated first hydration shell and a well-defined second shell. The application of advanced analysis tools such as the local-density-corrected three-body distribution revealed a minor structure-forming ability of Be^{2+} ion beyond the second hydration layer but denied the presence of a well-defined third hydration layer observed in a previous QM/MM MD simulation.[29] The comparative analysis of force constants, mean ligand residence times, and exchange processes give a clear order for structure-forming ability as $Mg^{2+} < Be^{2+} < Al^{3+}$.

Acknowledgment. Financial support for this work from the Austrian Science Foundation (FWF) and an Austrian Technology Grant (BMWKF/RFTE) for S.S.A. are gratefully acknowledged.

References and Notes

(1) Skilleter, D. N. *Chem.Br.* **1990**, *26* (1), 26–30.
(2) Wong, C. Y.; Woollins, J. D. *Coord. Chem. Rev.* **1994**, *130* (1−2), 243–273.
(3) Schmidbaur, H. *Coord. Chem. Rev.* **2001**, *215* (1), 223–242.
(4) Seidel, A. *Handbook of Inorganic Chemistry—Beryllium Supplement A1*; Springer: Berlin, 1986.
(5) Takagi, T.; Matsubara, K.; Takaoka, H. *J. Appl. Phys.* **1980**, *51* (10), 5419–5424.
(6) Greenfield, P. *Engineering Applications of Beryllium*; Mills: London, 1971.
(7) Fontenot, A.; Newman, L.; Kotzin, B. *Clin. Immunol.* **2001**, *100*, 4–14.
(8) Saltini, C.; Amicosante, M.; Franchi, A.; Lombardi, G.; Richeldi, L. *Eur. Respir. J.* **1998**, *12*, 1463–1475.
(9) Kuschner, M. *Environ. Health Perspect.* **1993**, *40* (6), 101–105.
(10) Schmidbaur, H. G. *Be-Org.* **1987**, *1*, 155.
(11) Kumberger, O.; Schmidbaur, H. *Chem. Unserer Zeit* **1993**, *27* (6), 310–316.
(12) Rossman, M.; Preuss, O.; Bowers, M. B. *Beryllium, Biomedical and Environmental Aspects*; Williams-Wilkins: Baltimore, MD, 1991.
(13) Wright, M. R. *An Introduction to Aqueous Electrolyte Solutions*; John Wiley: New York, 2007.
(14) Schwenk, C. F.; Hofer, T. S.; Rode, B. M. *J. Phys. Chem. A* **2004**, *108*, 1509–1514.
(15) Dance, I.; Freeman, H. *Acta Crystallogr. B* **1969**, *25* (2), 304–310.
(16) Sikka, S. K.; Chidambaram, R. *Acta Crystallogr. B* **1969**, *25* (2), 310–315.
(17) Probst, M. M.; Yamaguchi, T.; Ohtaki, H.; Spohr, E.; Heinzinger, K.; Palinkas, G. *Z. Naturforsch.* **1986**, *41*, 1175–1185.
(18) Richens, D. T. *The Chemistry of Aqua Ions*; John Wiley: Chichester, U.K., 1997.
(19) Pigenet, C. *J. Raman Spectrosc.* **1982**, *13* (1), 66–77.
(20) Pittet, P. A.; Elbaze, G.; Helm, L.; Merbach, A. E. *Inorg. Chem.* **1990**, *29* (1), 1936–1942.
(21) Tulinsky, A.; Worthington, C. R. *Acta Crystallogr. B* **1959**, *12*, 626–634.
(22) Jeffrey, G. A.; Parry, G. S.; Mozzi, R. L. *J. Chem. Phys.* **1956**, *25* (5), 1024–1031.
(23) Marx, D.; Sprik, M.; Parrinello, M. *Chem. Phys. Lett.* **1997**, *273* (5−6), 360–366.
(24) Lin, H.; Truhlar, D. G. *Theor. Chem. Acc.* **2007**, *117*, 185–199.
(25) Warshel, A.; Levitt, M. *J. Mol. Biol.* **1976**, *103*, 227–249.
(26) Field, M. J.; Bash, P. A.; Karplus, M. *J. Comput. Chem.* **1990**, *11* (6), 700–733.
(27) Gao, J. *J. Am. Chem. Soc.* **1993**, *115*, 2930–2935.
(28) Bakowies, D.; Thiel, W. *J. Phys. Chem.* **1996**, *100*, 10580–10594.
(29) D'Incal, A.; Hofer, T. S.; Randolf, B. R.; Rode, B. M. *Phys. Chem. Chem. Phys.* **2006**, *8*, 2841–2847.
(30) Rode, B. M.; Hofer, T. S.; Randolf, B. R.; Schwenk, C. F.; Xenides, D.; Vchirawongkwin, V. *Theor. Chem. Acc.* **2006**, *115*, 77–85.
(31) Hofer, T. S.; Randolf, B. R.; Rode, B. M. *Solvation Effects on Molecules and Biomolecules*; Springer: Heidelberg, Germany, 2008.
(32) Tongraar, A.; Leidl, K. R.; Rode, B. M. *J. Chem. Phys.* **1998**, *102* (50), 10340–10347.
(33) Rode, B.; Hofer, T. S.; Kugler, M. D. *The Basics of Theoretical and Computational Chemistry*; Wiley: New York, 2006.
(34) Fatmi, M. Q.; Hofer, T. S.; Randolf, B. R.; Rode, B. M. *J. Chem. Phys.* **2005**, *123*, 4514–4521.
(35) Hofer, T. S.; Pribil, A. B.; Randolf, B. R.; Rode, B. M. *Chem. Phys.* **2008**, *349* (03), 182–185.
(36) Schwenk, C. F.; Loeffler, H. H.; Rode, B. M. *J. Chem. Phys.* **2001**, *115*, 10808–10813.
(37) Schwenk, C. F.; Rode, B. M. *J. Chem. Phys.* **2003**, *119*, 9523–9531.
(38) Hofer, T. S.; Randolf, B. R.; Rode, B. M. *Phys. Chem. Chem. Phys.* **2005**, *7*, 1382–1387.
(39) Hofer, T. S.; Randolf, B. R.; Rode, B. M. *J. Chem. Phys.* **2005**, *26*, 949–956.
(40) Hofer, T. S.; Rode, B. M. *J. Phys. Chem.* **2004**, *121*, 6406–6411.
(41) Hofer, T. S.; Rode, B. M. *Chem. Phys.* **2005**, *312*, 81–88.
(42) Hofer, T. S.; Randolf, B. R.; Rode, B. M. *J. Am. Chem. Soc.* **2005**, *127* (41), 14231–14238.
(43) Hofer, T. S.; Scharnagl, H.; Randolf, B. R.; Rode, B. M. *Chem. Phys.* **2006**, *327* (1), 31–42.
(44) Hofer, T. S.; Randolf, B. R.; Rode, B. M. *J. Phys. Chem. B* **2006**, *110* (41), 20409–20417.
(45) Hofer, T. S.; Randolf, B. R.; Rode, B. M. *J. Phys. Chem. B* **2008**, *112* (37), 11726–11733.
(46) Hofer, T. S.; Shah, S. A. A.; Randolf, B. R.; Rode, B. M.; Persson, I. *Chem. Phys. Lett.* **2007**, *445* (4), 193–197.
(47) Rode, B. M.; Hofer, T. S. *Pure Appl. Chem.* **2006**, *78* (3), 525–539.
(48) Pribil, A. B.; Hofer, T. S.; Randolf, B. R.; Rode, B. M. *J. Comput. Chem.* **2008**, *29* (14), 2330–2334.
(49) Pribil, A. B.; Hofer, T. S.; Randolf, B. R.; Rode, B. M. *Chem. Phys.* **2008**, *346*, 182–185.
(50) Fatmi, M. Q.; Hofer, T. S.; Randolf, B. R.; Rode, B. M. *J. Comput. Chem.* **2007**, *28*, 1704–1710.
(51) Allen, M. P.; Tildesley, D. J. *Computer Simulation of Liquids*; Oxford Science Publications: Oxford, U.K., 1990.
(52) Krumhansl, J. A.; Wang, S. S. *J. Chem. Phys.* **1972**, *56*, 2034–2041.
(53) Tanaka, M.; Fukui, Y. *Prog. Theor. Phys.* **1975**, *53*, 1547–1565.
(54) Bhattacharjee, A.; Hofer, T. S.; Rode, B. M. *Phys. Chem. Chem. Phys.* **2008**, *10*, 6653–6657.
(55) Helm, L.; Merbach, A. *Coord. Chem. Rev.* **1999**, *187* (1), 151–181.
(56) Rode, B. M.; Schwenk, C. F.; Hofer, T. S.; Randolf, B. R. *Coord. Chem. Rev.* **2005**, *249*, 2993–3006.
(57) Scott, A. P.; Radom, L. *J. Phys. Chem.* **1996**, *100*, 16502–16513.
(58) DeFrees, D. J.; McLean, A. D. *J. Chem. Phys.* **1985**, *82* (1), 333–341.
(59) Berendsen, H. J.; Grigera, J. R.; Straatsma, T. P. *J. Phys. Chem.* **1987**, *91*, 6269–6271.
(60) Stillinger, F. H.; Rahman, A. *J. Chem. Phys.* **1978**, *68*, 666–670.
(61) Bopp, P.; Jansco, G.; Heinzinger, K. *Chem. Phys. Lett.* **1983**, *98*, 129–133.
(62) Martinez, J. M.; Pappalardo, R. R.; Marcos, E. S. *J. Am. Chem. Soc.* **1999**, *121*, 3175–3184.
(63) Tongraar, A.; Rode, B. M. *Chem. Phys. Lett.* **2005**, *409*, 304–309.
(64) Xenides, D.; Randolf, B. R.; Rode, B. M. *J. Mol. Liq.* **2006**, *123*, 61–67.
(65) Bard, A. J.; Parsons, R.; Jordan, J. *Standard Potentials in Aqueous Solution*; CRC Press: New York, 1985.
(66) Schwenk, C. F.; Rode, B. M. *Pure Appl. Chem.* **2004**, *76*, 37–47.
(67) Remsungnen, T.; Rode, B. M. *Chem. Phys. Lett.* **2003**, *367*, 586.
(68) Stangret, J.; Gampe, T. *J. Phys. Chem. A* **2002**, *106*, 5393–5402.
(69) Bischof, G.; Silbernagl, A.; Hermansoon, K.; Probst, M.; Sikka, S. K.; Chidambaram, R. *Int. J. Quantum Chem.* **1997**, *65*, 803–816.
(70) Mason, P.; Ansell, S.; Neilson, G.; Brady, J. *J. Phys. Chem. B* **2008**, *112* (7), 1935–1939.
(71) Tongraar, A.; Rode, B. M. *Chem. Phys. Lett.* **2001**, *346*, 485–491.
(72) Tongraar, A.; Rode, B. M. *Chem. Phys. Lett.* **2005**, *409*, 304–309.
(73) Hofer, T. S.; Randolf, B. R.; Rode, B. M. *Chem. Phys. Lett.* **2006**, *422*, 492–495.
(74) Scott, A. P.; Radom, L. *J. Phys. Chem.* **1996**, *100*, 16502–16513.
(75) DeFrees, D. J.; McLean, A. D. *J. Chem. Phys.* **1985**, *82*, 333–341.

JP903536K